RESEARCH ARTICLE

Insulin-like growth factor 1 partially rescues early developmental defects caused by SHANK2 knockdown in human neurons

Shu-Ting Chen[1, #], **Wan-Jing Lai**[1, 2, #], **Wei-Jia Zhang**[1], **Qing-Pei Chen**[1], **Li-Bing Zhou**[1], **Kwok-Fai So**[1], **Ling-Ling Shi**[1, 3, 4, *]

1 Guangdong-Hong Kong-Macau Institute of CNS Regeneration, Ministry of Education CNS Regeneration Collaborative Joint Laboratory, Jinan University, Guangzhou, Guangdong Province, China

2 Clinical Medicine, Jinan University, Guangzhou, Guangdong Province, China

3 Department of Psychiatry, the First Affiliated Hospital of Jinan University, Guangzhou, Guangdong Province, China

4 Co-innovation Center of Neuroregeneration, Nantong University, Nantong, Jiangsu Province, China

Funding: *This study was supported by the National Natural Science Foundation of China, No. 81771222 (to LLS); the Natural Science Foundation of Guangdong Province of China, No. 2019A1515011316 (to LLS); the National Key Research and Development Program of China, Stem Cell and Translational Research, No. 2017YFA0105102 (to LLS); the Guangzhou Science and Technology Innovation Development Special Fund Project of China, No. 201804010212 (to LLS); the Program of Introducing Talents of Discipline to Universities of China, No. B14036 (to KFS).*

Graphical Abstract

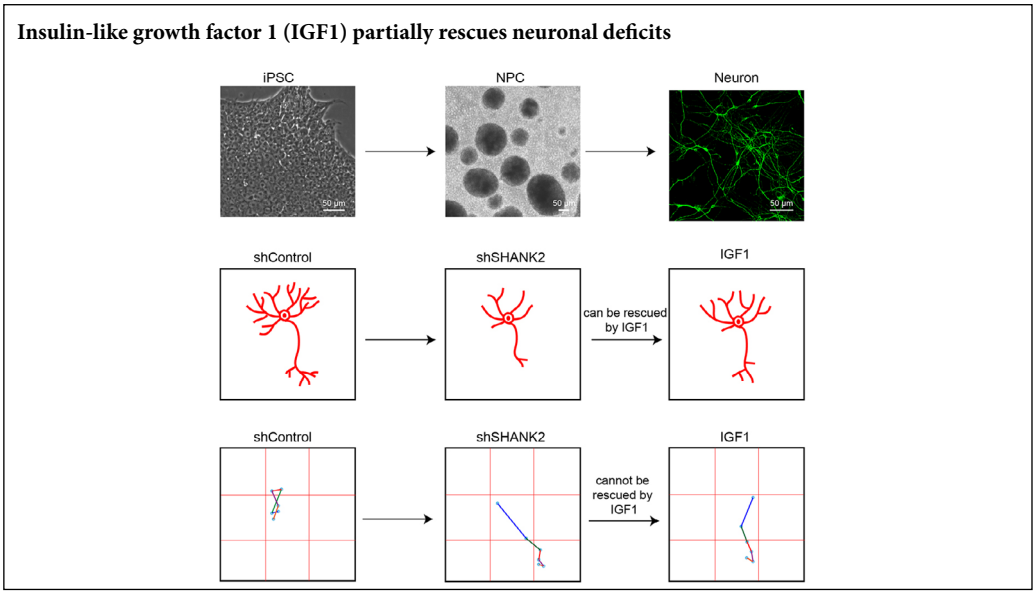

Correspondence to:
Ling-Ling Shi, MD, PhD, tlingshi@jnu.edu.cn.

#Both authors contributed equally to this work.

orcid:
0000-0003-4225-209X (Ling-Ling Shi)

doi: *10.4103/1673-5374.285002*

Received: *February 21, 2020*
Peer review started: *February 22, 2020*
Accepted: *April 1, 2020*
Published online: *June 19, 2020*

Abstract

SHANK2 is a scaffold protein that serves as a protein anchor at the postsynaptic density in neurons. Genetic variants of SHANK2 are strongly associated with synaptic dysfunction and the pathophysiology of autism spectrum disorder. Recent studies indicate that early neuronal developmental defects play a role in the pathogenesis of autism spectrum disorder, and that insulin-like growth factor 1 has a positive effect on neurite development. To investigate the effects of SHANK2 knockdown on early neuronal development, we generated a sparse culture system using human induced pluripotent stem cells, which then differentiated into neural progenitor cells after 3–14 days in culture, and which were dissociated into single neurons. Neurons in the experimental group were infected with shSHANK2 lentivirus carrying a red fluorescent protein reporter (shSHANK2 group). Control neurons were infected with scrambled shControl lentivirus carrying a red fluorescent protein reporter (shControl group). Neuronal somata and neurites were reconstructed based on the lentiviral red fluorescent protein signal. Developmental dendritic and motility changes in $VGLUT1^+$ glutamatergic neurons and TH^+ dopaminergic neurons were then evaluated in both groups. Compared with shControl $VGLUT1^+$ neurons, the dendritic length and arborizations of shSHANK2 $VGLUT1^+$ neurons were shorter and fewer, while cell soma speed was higher. Furthermore, dendritic length and arborization were significantly increased after insulin-like growth factor 1 treatment of shSHANK2 neurons, while cell soma speed remained unaffected. These results suggest that insulin-like growth factor 1 can rescue morphological defects, but not the change in neuronal motility. Collectively, our findings demonstrate that SHANK2 deficiency perturbs early neuronal development, and that IGF1 can partially rescue the neuronal defects caused by SHANK2 knockdown. All experimental procedures and protocols were approved by the Laboratory Animal Ethics Committee of Jinan University, China (approval No. 20170228010) on February 28, 2017.

Key Words: *cells; factor; growth; in vitro; model; neural differentiation; neurogenesis; plasticity*

Chinese Library Classification No. *R459.9; R363; R364*

Introduction

Autism spectrum disorder is a series of neurodevelopmental disorders characterized by deficits in cognition, social communication, reciprocal interactions and stereotypic behaviors (Geschwind, 2009). Genome-wide association studies have identified hundreds of rare, highly penetrant mutations and genomic imbalances in patients with autism spectrum disorder, including in the SHANK family of proteins (Berkel et al., 2010; Chilian et al., 2013; Turner et al., 2017). SHANK2 (also known as CortBP1 and ProSAP1) is a scaffold protein that serves as an anchor at the post synaptic density in excitatory neurons (Du et al., 1998; Sheng & Kim, 2000; Boeckers et al., 2001), where it interacts with various post synaptic density proteins through several domains, hinting at its key role in synaptic development and function (Tu et al., 1999; Sala et al., 2001; Hayashi et al., 2009; Grabrucker et al., 2011). SHANK2-deficient mice exhibit autistic-like behaviors, including reduced social interaction, impaired social communication, stereotyped behaviors, with or without hyperactivity, anxiety-like behaviors, and impaired motor learning and coordination (Schmeisser et al., 2012; Won et al., 2012; Ha et al., 2016; Peter et al., 2016; Kim et al., 2018). SHANK2 knockout mice show fewer dendritic spines, decreased synapse density, and a reduction in the frequency or amplitude of excitatory postsynaptic currents *in vivo* (Schmeisser et al., 2012; Won et al., 2012). In addition to impaired synaptic function, *in vitro* experiments have revealed disturbances in the length of neurites and in dendritic arborization, as well as decreased spine volume in cultured neurons with SHANK2 knockdown (Luo et al., 2018; Zaslavsky et al., 2019).

Recent studies show that loss of SHANK proteins impairs early neuronal development (Kathuria et al., 2018; Huang et al., 2019; Zaslavsky et al., 2019). Kathuria et al. (2018) discovered that induced pluripotent stem cell (iPSC)-derived placodal neurons containing a SHANK3 mutation from autism spectrum disorder patients display smaller cell bodies, more branched neurites, and reduced motility during early development. We independently demonstrated morphological deficits and synaptic transmission failure in immature SHANK3 knockdown iPSC-derived neurons (Huang et al., 2019). Given that SHANK protein family members have similar structure and function (Lim et al., 1999; Monteiro and Feng, 2017) and all play important roles in early development in different cell types, in concurrence with the early onset of autism spectrum disorder (Courchesne et al., 2007), we hypothesized that SHANK2 deficiency will have a significant impact on neurite outgrowth, dendritic arborization and motility in neurons at the early developmental stage.

Early interventions to restore synaptic function and promote neurogenesis with insulin-like growth factor 1 (IGF1) have been effective in improving behavioral abnormalities and rescuing neuronal phenotypes in several models of neurodevelopmental disorders (Marchetto et al., 2010; Shcheglovitov et al., 2013; Castro et al., 2014). IGF1 restores synaptic transmission in neurons from 22q13 deletion syndrome patients by increasing the number of AMPA and NMDA receptors (Shcheglovitov et al., 2013). IGF1 can also rescue Rett syndrome phenotypes by increasing glutamatergic synapse number (Marchetto et al., 2010; Castro et al., 2014).

Recent studies of SHANK-related neurodevelopmental disorders have mainly focused on abnormal synaptogenesis and synaptic dysfunction (Zhou et al., 2016; Shi et al., 2017; Fourie et al., 2018; Wegener et al., 2018). However, other aspects of early neuronal development before circuit formation, including neuronal morphogenesis and motility, have largely been ignored. Therefore, in this study, we used iPSC-derived cells to create a translatable disease-in-a-dish neuronal model to unravel the effect of SHANK2 deficiency. Furthermore, we examined the motility of immature neurons, which is critical for brain circuit establishment. We also treated shSHANK2 and control neurons with IGF1 over the course of early development to assess any improvements in dendritic length, neurite arborization, and neuronal motility.

Materials and Methods

Culture and induced neural differentiation of iPSCs

All experimental procedures and protocols were approved by the Laboratory Animal Ethics Committee of Jinan University, China (approval No. 20170228010) on February 28, 2017. Human urine epithelium-derived cells were reprogrammed into iPSCs (Wang et al., 2013). The cellular experiments were approved by the Medical Ethics Committee of the First Affiliated Hospital of Jinan University of China on February 25, 2017. The iPSC cells used were provided by the Chinese Academy of Sciences (Pei lab). The iPSCs were cultured in six-well plates coated with Matrigel and maintained in mTeSR medium (Cat# 085851; Stem cell Technologies, Vancouver, BC, Canada). The medium was added to each well and refreshed every day. When cell density reached 70–80% confluence, colonies were dissociated using PBS containing EDTA (0.5 mM, Cat# AM9261; Thermo Fisher Scientific, Waltham, MA, USA) and plated onto Matrigel (Cat# 354277; BD, Franklin Lakes, NJ, USA)-coated plates at a 1:3 dilution. The iPSC colonies were propagated for 2–3 passages. After reaching 95% confluence, the cells were digested with EDTA, and passed to Matrigel-coated 12-well plates. With cells at 100% confluence, the medium was changed to N2/B27 containing two inhibitors (5 μM dorsomorphin and 5 μM SB431542; Cat# S7840 and S1067; Selleck, Houston, TX, USA). Dorsomorphin and SB431542 effectively inhibit the SMAD signaling pathway by blocking phosphorylation of ALK4, ALK5 and ALK7 receptors, thereby improving the efficiency of neural induction. The medium was supplemented with inhibitors and replaced every other day for 7 days. On day 8, the cells were mechanically scraped onto Matrigel-coated six-well plates with neural proliferation system I medium (N2/B27, Cat# 17502-048 and 17504-044; Thermo Fisher Scientific). The medium was replaced every other day, and the cells differentiated into neural rosettes. On day 16, the cells were mechanically scraped and transferred to T25 flasks and cultured with neural proliferation system II (N2/B27 + 20 ng/mL bFGF + 20 ng/mL EGF, Cat# PHG0266 and PHG0315; Thermo Fisher Scientific). Thereafter, the rosettes were manually dissociated to purify

neural progenitor cells (NPC). Immunocytochemistry was performed for the pluripotency-associated factors OCT4 and SSEA4, and for the NPC markers Nestin and SOX2.

To begin neuronal differentiation, NPCs were expanded for three passages with Accutase (Cat# A1110501; Thermo Fisher Scientific). For morphological analysis and time-lapse imaging experiments, the cells were infected with shControl or shSHANK2 lentivirus for 6 hours (1×10^8 TU/mL) after NPC dissociation, and then the lentivirus was washed out. Red fluorescent protein (RFP) expression was induced by addition of doxycycline (1 μg/mL) to the medium after washout of the lentivirus. NPCs were further dissociated into single cells on day 3, and cultured with a glial cell feeder layer (prepared from rat astrocytes, P0–P3) at a density of 5×10^5 cells per well on glass coverslips. The first day of induction on coverslips was defined as day 0. The medium was switched to neuron differentiation medium (N2/B27, Thermo Fisher Scientific; 1 μM dibutyryl-cAMP, Cat# D0627, Sigma-Aldrich, St. Louis, MO, USA; 20 ng BDNF, Cat# 450-02, PeproTech, Rocky Hill, NJ, USA). The plates were maintained at 37°C in a humidified incubator with 95% air and 5% CO_2. In the rescue experiment, IGF1 (200 ng/mL, Cat# 291-G1-200; R&D Systems, Minneapolis, MN, USA) was added to the differentiation medium every day after infection, with approximately 25% of the medium replaced every other day. Day 3 to day 14 was defined as the early neuronal developmental stage.

Immunofluorescence and morphological analysis

Cells on day 9 were used for immunofluorescence staining and morphological analysis. Dendritic length and arborizations were analyzed in neurons that were sparsely infected with lentivirus (1×10^8 TU/mL) containing a tetracycline-controlled RFP expression sequence to obtain fluorescent images. Neurons grown on coverslips were collected on day 9 and fixed with 4% paraformaldehyde for 30 minutes, washed with PBS, and blocked with 1% bovine serum albumin (Cat# WXBC1064V; Sigma-Aldrich) in PBS. Primary antibodies were diluted in 1% bovine serum albumin in PBS with 0.3% Tween-20 (Cat# T8220; Solarbio, Beijing, China) and applied overnight at 4°C. The cells were stained with the following antibodies: mouse OCT4 (octamer-binding transcription factor 4, an iPSC marker; 1:200, Cat# 6765-100; BD Pharmingen, Franklin Lakes, NJ, USA), mouse SSEA4 (stage-specific embryonic antigen-4, an iPSC marker; 1:100; Cat# 41-4000; Invitrogen, Rockford, AL, USA), mouse SOX2 (SRY-box transcription factor 2, an NPC marker; 1:500; Cat# MAB2018; R&D Systems), rabbit Nestin (an NPC marker; 1:1000; Cat# ABD9; Millipore, Darmstadt, Germany), rabbit microtubule-associated protein 2 (MAP2, a dendritic marker; 1:1000; Cat# AB5622; Millipore), mouse VGLUT1 (anti-vesicular glutamate transporter 1, a glutamatergic neuron marker; 1:250; Cat#MAB5502; Millipore), rabbit tyrosine hydroxylase (TH, a dopaminergic neuron marker; 1:1000; Cat# AB152; Millipore), and rabbit SHANK2 (1:1000; Cat# 162202; Synaptic Systems, Göttingen, Germany). Secondary antibodies, including donkey anti-mouse Alexa-488 (1:1000; Cat# R37114; Invitrogen) and donkey anti-mouse Alexa-546 (1:1000; Cat# A10036; Invitrogen), were used along with DAPI (1:4000; Cat#D1306; Thermo Fisher Scientific), and were diluted (1:500) in PBS and applied for 1 hour at room temperature. Co-localization of SHANK2 in different types of neurons was accessed by immunofluorescence intensity. Images of neurons were visualized (Imager Z2, Zeiss, Jena, Germany) on a laser scanning confocal microscope equipped with 405/488/555/639 nm lasers (Axiocam 506 mono; Zeiss). Morphology, including neurite length and complexity of neurite arborization (represented by number of branch intersections), were tracked and analyzed by Sholl analysis using Neurolucida 360 software (MBF Bioscience, Williston, OH, USA).

Western blot assay

Western blot assay was performed on day 9. Cells grown in 32 mm dishes were washed twice with PBS (1 mL/well), and then lysed in a standard RIPA buffer (Cat# 89900; Thermo Fisher Scientific) containing a protease inhibitor cocktail (50:1, Cat# 539137-10VL, Millipore). Cells were collected with a cell scraper (NEST Biotechnology, Wuxi, China). The cell suspension was kept on ice for 30 minutes, and then centrifuged at 4°C at $6526 \times g$ for 15 minutes. Protein concentrations were measured using the Pierce BCA Protein Assay Kit (Cat# 23225; Thermo Fisher Scientific). Protein samples were mixed with 10× loading buffer (Cat# PV015; Beyotime, Shanghai, China), heated for 8 minutes at 90°C, separated by 8% sodium dodecyl sulfate-polyacrylamide gel electrophoresis, and transferred to a polyvinylidene difluoride membrane (Cat# IPVH00010; Millipore). Membranes were blocked in 5% bovine serum albumin for 1 hour at room temperature, and then incubated with the primary antibodies for 12 hours at 4°C. The primary antibodies were as follow: rabbit SHANK2 (1:1000; Cat# 162202; Synaptic Systems, Göttingen, Germany), rabbit GAPDH (1:4000; Cat# D110016; BBI Life Sciences, Shanghai, China), and rabbit GAPDH (housekeeping gene as control; 1:4000; Cat# D110016; BBI Life Sciences). The following day, the membranes were washed three times with phosphate-buffered saline containing 0.4% Tween-20 (Solarbio) for 8 minutes, incubated with anti-rabbit horseradish peroxidase-linked secondary IgG antibodies (1:4000; Cat# 7074P2; Cell Signaling, Boston, MA, USA) for 1.5 hours at room temperature, and then washed five times for 8 minutes each. Protein signals were visualized using the Chemi-Doc Touch Imaging System (Bio-Rad, Hercules, CA, USA). The gray values of protein bands were analyzed with ImageJ software (win 64, National Institutes of Health, Bethesda, MD, USA), and shSHANK2 was normalized to shControl.

Calcium imaging

Calcium imaging was performed on day 14. Cells were treated with 5 μM Fluo-4 AM (Cat# F312; Dojindo Laboratories, Kyushu, Japan) and incubated for 30 minutes at 37°C in a 5% CO_2 incubator. After incubation, the cells were perfused with low-potassium solution containing 125 mM NaCl, 3 mM KCl, 1.2 mM NaH_2PO_4, 25 mM $NaHCO_3$, 1 mM $MgCl_2$, 2 mM $CaCl_2$ and 10 mM D-glucose, pH 7.2–7.4, and then

imaged with a Ca^{2+} imaging system (Observer Z1, Zeiss). The Fluo-4 AM fluorescence was detected at a wavelength of 470 nm. After 3 minutes, the perfusion solution was replaced by high-potassium solution containing 68 mM NaCl, 60 mM KCl, 1.2 mM NaH_2PO_4, 25 mM $NaHCO_3$, 1 mM $MgCl_2$, 2 mM $CaCl_2$ and 10 mM D-glucose, pH 7.2–7.4, for 6 minutes. High-potassium solution was used to stimulate calcium release in neurons, and the calcium ion concentration in neurons was measured by fluorescence intensity. After 6 minutes, the high-potassium solution was washed out with low-potassium solution. Changes in calcium ion concentration were expressed as changes in Fluo-4 AM fluorescence intensity. The Fluo-4 AM fluorescence intensity of the RFP signal in cells was measured with imageJ to compare neuronal activity between shControl and shSHANK2.

Virus infection

The shSHANK2 virus (V2THS_192790) has been described previously. The mature antisense product is 5′-TCT CAG CGC GGG AGG G-3′, while the non-targeting TRIPZ lentivirus inducible control contained the non-silencing scrambled shRNAmir sequence (Dharmacon, Inc., Austin, TX, USA). Neurons infected with the shSHANK2 virus were termed the shSHANK2 group, and those infected with the shRNAmir control were termed the shControl group.

Neuronal motility analysis using time-lapse imaging

Neuronal motility analysis by time-lapse imaging was performed on day 5. Single-cell NPCs were infected with shControl or shSHANK2 lentivirus, together with a CaMKII-GFP reporter to identify glutamatergic neurons by live cell imaging. The cells were plated at a density of 5×10^5 cells per well on glass coverslips coated with a glial cell feeder layer. After 5 days of culture, the coverslips were transferred to 32 mm glass bottom dishes and placed in an environmentally controlled stage. We chose a 10× field where most cells expressed both RFP and green fluorescent protein (GFP) signals. Time-lapse images of neurons were taken every 10 minutes for a few hours on a Zeiss Observer Z1 (Zeiss). Each target neuron was then tracked and measured using Imaris (Bitplane, Zurich, ZH, Switzerland). Cell soma motility (μm/hour) was measured as directional velocity; distance between the centers of cell soma (μm) was divided by the time period (hour).

Statistical analysis

Statistical analysis was performed using GraphPad Prism 7.0 software (GraphPad, San Diego, CA, USA), and the results were expressed as the mean ± SEM. Differences were analyzed by parametric statistical analysis (Student's *t*-test or two-way repeated measures analysis of variance) between shControl and shSHANK2 groups. A value of $P < 0.05$ was considered statistically significant.

Results

Generation of human iPSC-derived neuron model

A sparse culture system based on the human iPSC-iNeuron model was used to investigate the functional role of SHANK2 in early neuronal development. The human iPSC-iNeuron model was produced using a protocol previously described by our group (Kang et al., 2017; Huang et al., 2019). The human iPSCs used in this experiment were positive for the iPSC-specific markers OCT4 and SSEA4 (**Figure 1A**), and differentiated into cells positive for the NPC-specific markers SOX2 and Nestin (**Figure 1B**). The NPCs were directly plated on glass coverslips coated with Matrigel and a mouse astrocyte feeder layer in 24-well plates. The neuronal subtype marker proteins TH and VGLUT1 were detected by immunohistochemistry together with MAP2 (**Figure 1C** and **D**). The labeling results showed that multiple types of neurons were successfully induced from human iPSCs.

Effects of SHANK2 knockdown on neuronal morphogenesis in a sparse culture system

As the cell density of a neuron culture system affects neuronal morphology and synaptic functional maturation, we used a sparse culture system in which NPCs were transfected with lentivirus carrying shSHANK2 and RFP and then cultured sparsely on a plate with an enriched neuron feeder. The lentiviral RFP signal was examined 3 days post infection. Knockdown efficiency was verified by immunocytochemical staining of cultured neurons (**Figure 2A** and **B**). The fluorescence intensity of the SHANK2 signal was reduced in the neurites (**Figure 2C**) and somata (**Figure 2D**), compared with the control group. SHANK2 knockdown efficiency was estimated at approximately 60% in neurites and 45% in somata. Western blot assay (**Figure 2E**) and quantitative analysis of gray values (**Figure 2F**) showed significantly decreased SHANK2E protein levels in shSHANK2 neurons ($P = 0.0021$). Because a high concentration of lentivirus can result in a reduced neuronal survival rate, in turn affecting neuronal development, we used a 70% infection efficiency, in which SHANK2 knockdown efficiency was lower in western blot assay than in immunofluorescence.

To investigate the morphogenesis of excitatory neurons ($VGLUT1^+$) and putative dopamine neurons (TH^+) following SHANK2 knockdown, we tracked $VGLUT1^+$ and TH^+ neurons, reconstructed neuronal morphology, and quantified neurite complexity using Sholl analysis on day 9, a time period that represents the early developmental stage of neurons, as indicated by our pilot study. Here, we examined neurite outgrowth, dendritic length and the number of neurite branches based on the RFP signal. Dendrites were labelled by MAP2, while dopaminergic and glutamatergic neurons were labelled by TH and VGLUT1, respectively (**Figure 3A** and **B**). Student's *t*-test and two-way repeated measures analysis of variance revealed that SHANK2 knockdown caused significant reductions in dendritic length ($P = 0.0263$) and neurite complexity ($P < 0.0001$) in $VGLUT1^+$ neurons (**Figure 3E** and **F**), without significantly affecting TH^+ neurons (**Figure 3C** and **D**).

Neuronal motility defect in shSHANK2 immature neurons *in vitro*

Because SHANK2 knockdown causes morphological chang-

es in VGLUT1$^+$ excitatory neurons, we examined whether it would also have an impact on neuronal motility, another critical process for proper neuronal circuit formation. We monitored cell soma movement by time-lapse imaging of iPSC-iNeurons 5 days post infection with lentivirus expressing shSHANK2 and a CaMKII promoter-driven GFP reporter (to specifically monitor CaMKII neurons). The analysis revealed that soma velocity of CaMKII$^+$ iPSC-iNeurons in the shSHANK2 group was significantly increased compared with the shControl group ($P = 0.0009$; **Figure 4C**).

IGF1 rescues morphological defects, but not neuronal motility, in SHANK2 knockdown neurons

Given the morphological and motility defects in iPSC-derived glutamatergic neurons following SHANK2 knockdown, both shControl and shSHANK2 glutamatergic neurons were treated with IGF1, 1 day after plating (**Figure 5A** and **B**). Student's *t*-test and two-way repeated measures analysis of variance revealed that both dendritic length ($P < 0.0001$) and arborization ($P < 0.0001$) phenotypes in shSHANK2 glutamatergic neurons were completely rescued by IGF1 treatment (**Figure 5D** and **E**). These results show that the morphologic defects in shSHANK2 neurons can be rescued by early intervention with IGF1. Moreover, dendritic length also improved in shControl neurons following IGF1 intervention ($P = 0.0120$; **Figure 5E**), while neurite complexity showed no significant change ($P = 0.5442$; **Figure 5C**).

Because morphologic deficits caused by SHANK2 knockdown could be rescued by IGF1, we next examined whether IGF1 could rescue the neuronal motility defect in CaMKII$^+$ shSHANK2 neurons. Student's *t*-test showed that IGF1 had no effect on cell motility in shControl neurons ($P = 0.1448$) or shSHANK2 neurons ($P = 0.4327$; **Figure 6C**).

Impaired neuronal function in SHANK2 knockdown neurons

Though our experiments focused more on early neuronal development of SHANK2-deficient neurons, we also assessed function 2 weeks post infection by calcium imaging. Before stimulation with high-K$^+$, neurons in both groups were normalized, and displayed a similar low baseline fluorescence. An increase in the intensity exceeding fluctuation of the baseline was identified as a response. Two-way repeated measures analysis of variance showed that the fluorescence intensity of Fluo-4 AM was significantly lower in shSHANK2 neurons than in shControl neurons after high-K$^+$ stimulation ($P < 0.0001$; **Figure 7C**), suggesting that SHANK2 deficiency impairs neuronal function.

Discussion

During early neural development, neurogenesis and neuronal migration are important physiological processes that lay the foundation for synaptic connections and functional neural circuit formation (Lee et al., 2016; Garcia-Gonzalez et al., 2017; Lim et al., 2018). In addition to abnormal neurite outgrowth, aberrant neuronal migration resulting from molecular machinery defects is also considered an important pathogenetic mechanism in autism spectrum disorder (Wegiel et al., 2010; Pan et al., 2019). In current studies of neurodevelopmental disorders related to Shankopathies, much attention has been given to the role of abnormal synaptogenesis leading to synaptic dysfunction. However, whether abnormal neuronal motility at the cellular level contributes to the dysfunctional brain circuitry in SHANK2 knockdown models has been largely ignored.

Here, we investigated whether SHANK2 knockdown affects the growth and motility of neurons in the early developmental stage using an iPSC-iNeuron model. SHANK2 knockdown resulted in reduction of dendritic length and neurite complexity in VGLUT1$^+$ neurons, and caused a marked increase in cell body motility in CaMKII shSHANK2 neurons. Furthermore, fluorescence calcium imaging was used to assess neuronal activity and functionality of mature neurons (Kamijo et al., 2018). This analysis showed that the calcium increase evoked by high-K$^+$ was significantly weaker in neurons with SHANK2 knockdown. Disturbances in calcium signaling have been correlated with several brain disorders (for review, see Pchitskaya et al., 2018), highlighting its importance in neurotransmitter release and activity-dependent synaptic plasticity (Neher and Sakaba, 2008; Mateos-Aparicio and Rodriguez-Moreno, 2020).

SHANK2 is a scaffold protein that functions as an anchor at the postsynaptic density, and has been shown to be tightly linked to neuropsychiatric and neurodevelopmental diseases in animals and cell culture models (Berkel et al., 2012; Sala et al., 2015; Eltokhi et al., 2018; Zaslavsky et al., 2019). Most previous studies on SHANK2 using *in vivo* and *in vitro* models explored the effects of truncated SHANK2 on synaptogenesis and synaptic function in mature neurons. SHANK2 mutants exhibit abnormalities in the NMDA/AMPA ratio in synapses, defects in synaptic transmission in different types of neurons, and electrophysiological perturbations in various brain regions (Schmeisser et al., 2012; Won et al., 2012; Lim et al., 2017; Pappas et al., 2017; Wegener et al., 2018).

Consistent with previous *in vitro* studies of cultured mature neurons by Schimeisser et al. (2012) and Luo et al. (2018), we observed a striking reduction in neurite arborization and dendritic length in glutamatergic, but not dopaminergic, neurons. This suggests that SHANK2 has a role in the regulation of neuronal structure in early morphogenesis, and that this is a cell-type-specific phenomenon. This finding provides insight into the pathogenetic basis of impaired hippocampal glutamatergic transmission and NMDAR-dependent synaptic plasticity in SHANK2 mutants (Schmeisser et al., 2012; Won et al., 2012; Chung et al., 2019).

Early intervention by restoring synaptic function and promoting neurogenesis with IGF1 has been shown effective in improving behavioral abnormalities and rescuing neuronal phenotypes in several neurodevelopmental disorder models (Marchetto et al., 2010; Shcheglovitov et al., 2013; Castro et al., 2014). Interestingly, IGF1 increased dendritic length and branching in shSHANK2 glutamatergic neurons, but did not affect cell soma speed. Why does IGF1 rescue morphological deficits, but not neuronal motility? Studies on the physiolog-

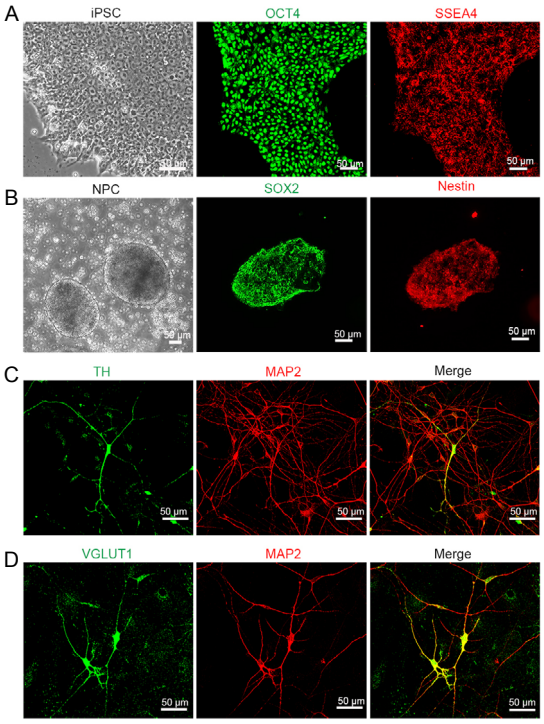

Figure 1 Immunofluorescence staining of human iPSC-derived neurons.

(A) Characterization of iPSCs positive for OCT4 and SSEA4. (B) NPCs induced from iPSCs were positive for SOX2 and Nestin. (C, D) Human neurons differentiated from NPCs were positive for TH or VGLUT1 after 9 days of culture, together with MAP2, suggesting that the NPCs could differentiate into multiple types of neurons. Scale bars: 50 μm. All images were captured by Imager Z2, Zeiss, and processed with Photoshop and Illustrator. iPSCs: Induced pluripotent stem cells; SSEA4: stage-specific embryonic antigen-4; SOX2: SRY (sex determining region Y)-box 2; NPC: neural progenitor cells; TH: tyrosine hydroxylase; VGLUT1: vesicular glutamate transporter 1; MAP2: microtubule-associated protein 2; OCT4: octamer-binding transcription factor 4.

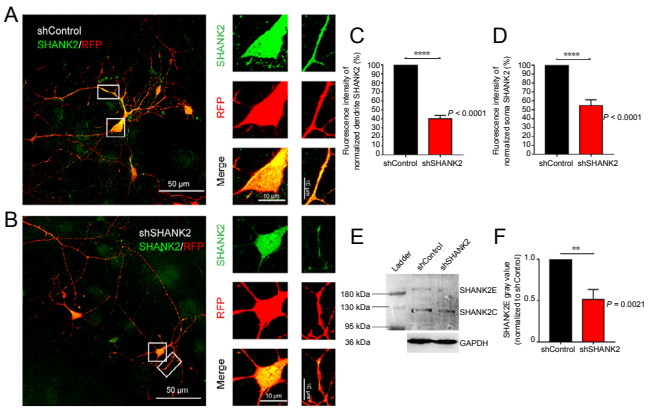

Figure 2 Efficient downregulation of SHANK2 in iPSC-derived neurons infected by shSHANK2 lentivirus.

(A, B) Immunofluorescence staining using anti-SHANK2 antibodies for SHANK2 protein in neurons infected by shControl or shSHANK2 viruses (RFP) on day 9. Scale bars: 50 μm. All images were captured by confocal microscope. (C, D) Fluorescence intensity of SHANK2 in the shSHANK2 group, normalized to the shControl group (%). Fluorescence intensity of SHANK2 was lower in shSHANK2 neurons than in shControl neurons in both dendrites and somata. Data are presented as the mean ± SEM. ****P < 0.0001; Student's t-test. n (shSHANK2) = 34 (neurite)/29 (soma); n (shControl) = 33 (neurite)/29 (soma). SHANK2 knockdown efficiency was estimated at approximately 60% in neurites and 45% in somata. (E) Western blot assay showing decreased SHANK2E protein levels in shSHANK2 neurons compared with shControl neurons, normalized to GAPDH. (F) Gray value of protein bands assessed with ImageJ shows a significant decrease in SHANK2E protein levels, normalized to GAPDH, in shSHANK2 neurons compared with shControl neurons. Data are presented as the mean ± SEM from three independent experiments. Student's t-test: **P < 0.01. GAPDH: Glyceraldehyde-3-phosphate dehydrogenase; RFP: red fluorescent protein.

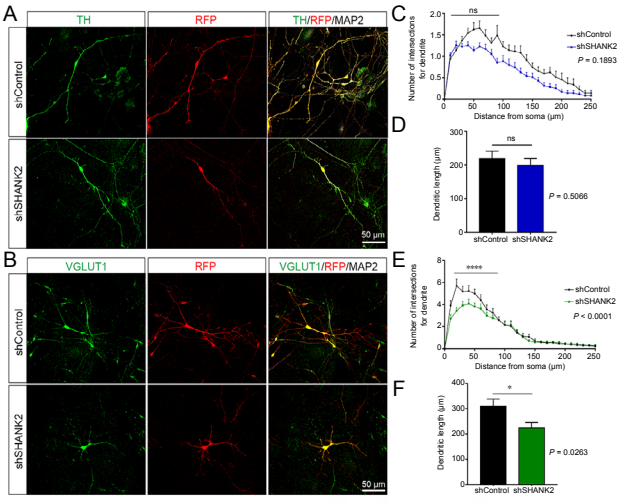

Figure 3 Distinct effects of SHANK2 downregulation on the morphology of VGLUT1$^+$ and TH$^+$ neurons.

(A, B) Immunofluorescence staining for TH (green), VGLUT1 (green) and MAP2 (white) in the two types of differentiated neurons. Scale bar: 50 μm. All images were captured by confocal microscope. The morphology of neurons was reconstructed with Neurolucida 360 and analyzed by Sholl analysis based on the RFP signal. (C) No significant difference was observed in the complexity of neurite arborization (represented by Y axis: number of branch intersections of dendrites) between shSHANK2 (n = 35) and shControl (n = 35) groups among TH$^+$ neurons. (D) No significant difference in dendritic length (μm) between shSHANK2 (n = 35) and shControl (n = 35) groups was detected in TH$^+$ neurons. (E) Complexity of neurite arborization (represented by Y axis: number of branch intersections of dendrites) was significantly decreased in the shSHANK2 group (n = 33) compared with the shControl group (n = 29) among VGLUT1$^+$ neurons. (F) Dendritic length (μm) was significantly decreased in the shSHANK2 group (n = 33) compared with the shControl group (n = 29) among VGLUT1$^+$ neurons. Data are presented as the mean ± SEM (Student's t-test and two-way repeated measures analysis of variance). *P < 0.05, ****P < 0.0001. ns: Not significant; RFP: red fluorescent protein; TH: tyrosine hydroxylase; VGLUT1: vesicular glutamate transporter 1.

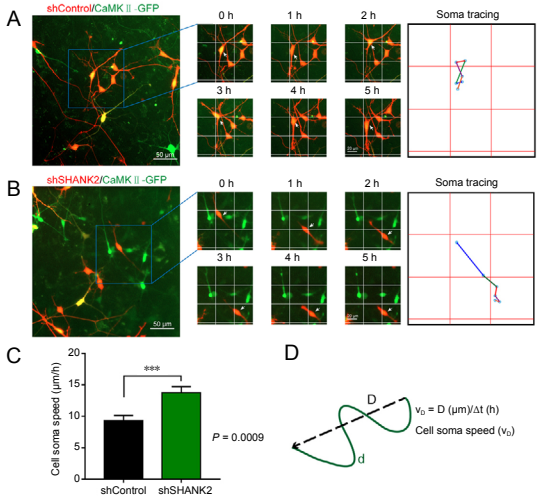

Figure 4 Abnormal neuronal motility in immature neurons after SHANK2 knockdown.

(A, B) Phase-contrast images of shControl and shSHANK2 neurons. Cell somata were tracked at 0, 1, 2, 3, 4 and 5 hours. The speed of the cell somata (white arrows) in neurons with both the lentivirus (RFP) and CaMKII (GFP) signal was analyzed with Imaris. Scale bar: 50 μm. All images were captured on an Observer Z1 microscope, Zeiss. (C) Cell soma speed (μm/h) was significantly increased in the shSHANK2 group (n = 41) compared with the shControl group (n = 35). (D) Cell soma speed was measured as directional velocity, distance from the beginning and end point of the soma center traced every 1 hour. Data are presented as the mean ± SEM (Student's t-test). ***P < 0.001. GFP: Green fluorescent protein; RFP: red fluorescent protein.

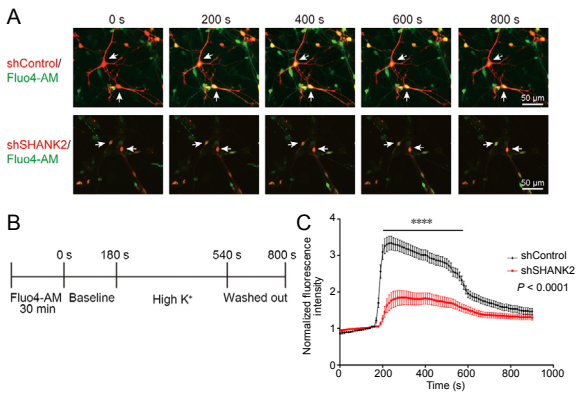

Figure 7 Calcium imaging of cultured neurons loaded with Fluo-4 AM before and after potassium stimulation.

(A) Relative intensity of Fluo-4 AM emissions was monitored in shSHANK2 and shControl neurons. Arrows show the calcium traces in cell soma together with RFP signal at 0, 200, 400, 600 and 800 seconds. Scale bars: 50 μm. Images were captured on an Observer Z1, Zeiss. (B) Protocol of calcium imaging. Cells were treated with 5 μM Fluo-4 AM and incubated for 30 minutes at 37°C in a 5% CO_2 incubator. High-potassium solution was added to stimulate calcium release in neurons for 6 minutes, and then washed out with low potassium solution. (C) Before the stimulation with high-K^+, neurons in both groups were normalized, and remained in the lowest level of fluorescence intensity with a similar baseline on average. An increase in the intensity exceeding fluctuation of the baseline was identified as a response. Fluorescence intensity of Fluo-4 AM was significantly lower in shSHANK2 neurons (n = 34) than in shControl neurons (n = 33) after potassium stimulation: ****P < 0.0001. Data are presented as the mean ± SEM (two-way repeated measures analysis of variance). RFP: Red fluorescent protein.

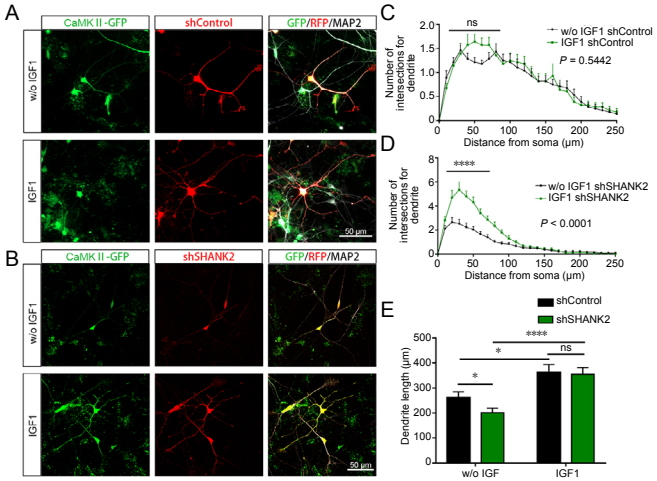

Figure 5 IGF1 rescues morphological defects in SHANK2 knockdown neurons.

(A, B) Immunofluorescence staining for MAP2 (white) in shControl and shSHANK2 neurons, accompanied with CaMKII-GFP (green) and lentivirus signal (red). Scale bar: 50 μm. All images were captured by confocal microscope. Neuronal morphology was reconstructed with Neurolucida 360 and analyzed by Sholl analysis based on the RFP signal. (C) No significant difference was observed in neurite arborization in the shControl group, with or without IGF1 treatment. (D) Complexity of neurite arborization was significantly increased in shSHANK2 neurons after treated with IGF1. (E) Dendritic length analysis in both groups, with and without IGF1 treatment. Dendritic length was significantly increased in shSHANK2 neurons given IGF1 treatment compared with without (w/o) IGF1 treatment. This phenomenon was also seen in shControl neurons. Statistical analysis of other comparisons: w/o IGF1: shControl (n = 27) *vs.* shSHANK2 (n = 28); IGF1: shControl (n = 26) *vs.* shSHANK2 (n = 23); P = 0.8645. Data are presented as the mean ± SEM (Student's t-test and two-way repeated measures analysis of variance). *P < 0.05, ****P < 0.0001. GFP: Green fluorescent protein; IGF1: insulin-like growth factor 1; ns: not significant; RFP: red fluorescent protein.

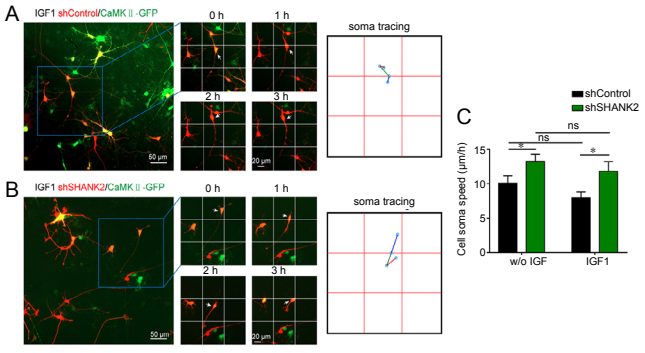

Figure 6 IGF1 does not rescue neuronal motility in SHANK2 knockdown neurons.

(A, B) Phase-contrast images of shControl and shSHANK2 neurons tracked at 0, 1, 2 and 3 hours. The speed of cell soma (white arrows) displaying both lentivirus (red) and CaMKII-GFP (green) signals was analyzed with Imaris. Original magnification: 10×. Scale bar: 50 μm. All images were captured on an Observer Z1, Zeiss. (C) Without IGF1 treatment, cell soma speed (μm/h) in the shSHANK2 group was significantly higher than in the shControl group. This difference persisted after IGF1 treatment. Within group comparison, IGF1 treatment did not significantly influence soma speed in either the shControl or shSHANK2 group. w/o IGF1: n (shControl) = 24, n (shSHANK2) = 32; IGF1: n (shControl) = 20, n (shSHANK2) = 14. Data are presented as the mean ± SEM (Student's t-test.). *P < 0.05. GFP: Green fluorescent protein; IGF1: insulin-like growth factor 1.

ical function of IGF1 in brain development show that global disruption of the IGF1 gene results in smaller neurons with fewer dendrites, branches and synapses (Cheng et al., 2001; Fuentes-Santamaria et al., 2019). IGF1 is a neurotrophic factor that supports neurogenesis and neuronal differentiation (Scolnick et al., 2008; Bianchi et al., 2017). Our current data suggest that the effect of IGF1 is global, as suggested by the increased dendritic length in IGF1-treated shControl neurons, concordant with the dendritic changes in mutant R841X and restored R841X-C neurons (Zaslavsky et al., 2019). Therefore, a novel drug may be administrated in combination with IGF1 to fully rescue the defect in shSHANK2 neurons.

Hyperactive neuronal migration remains in shSHANK2 neurons after IGF1 treatment. This warrants further investigation of the mechanisms by which SHANK2 knockdown turns off the static signal in neurons. A recent study demonstrates that another SHANK family member, SHANK3, is involved in integrin-extracellular matrix-mediated cell soma motility via the SPN terminal (Lilja et al., 2017). This study suggests an association between SHANK3 and neuronal dynamics, linking the protein to neurodevelopmental diseases. This study also suggests that the expression level of SHANK3 affects the activation-inactivation oscillatory state of integrin, which interacts with the extracellular matrix, thereby modulating the migration and dynamic behavior of cell bodies (Lilja et al., 2017). Collectively, these observations imply a close relationship between SHANK and neuronal motility. Therefore, it is important to identify drugs that rescue the various phenotypes caused by SHANK2 deficiency to advance therapies for neurodevelopmental disorders.

While the present study is the first to demonstrate that SHANK2 knockdown results in aberrant neuronal motility in the early developmental stage *in vitro*, there are some limitations. For example, the SHANK2 mutation was not derived from autism spectrum disorder or neuropsychiatric patients. Moreover, except for the relationship between the SHANK protein family and integrin, the mechanisms by which motility is affected by SHANK2 knockdown remain unclear, requiring further study. More importantly, the synaptic transmission alterations in glutamatergic SHANK2 knockdown neurons, such as AMPA and NMDA-dependent electrophysiological changes, as well as its reversibility via IGF1 intervention, were not assessed in our study.

In summary, SHANK2 downregulation in iPSC-derived human neurons perturbs neurite outgrowth and neuronal motility, manifested by decreased dendritic length and branch number, and increased somatic speed. IGF1 administration only rescued the morphological defects, and not the change in neuronal motility. Defects in early developmental processes have a wide range of consequences for the timely, coordinated establishment of connectivity of neuronal networks. Therefore, it is crucial to assess the reversibility and specificity of the varied perturbations to restore normal function in SHANK-related neurodevelopmental disorders. Drug candidates should target not only neurogenesis, but also early neuronal migration.

Acknowledgments: *We thank our lab "Guangdong-HongKong-Macau Institute of CNS Regeneration" for providing us platform to do scientific researches. We thank Prof. Duan-Qing Pei from Chinese Academy of Sciences for providing the iPSC cell lines used in the study.*

Author contributions: *Study design, manuscript writing: LLS; performance of cell culture experiment, live cell imaging, neural morphology reconstruction, and data analysis: STC, WJL; co-writing the initial draft of the manuscript: WJL, QPC and WJZ; critical revision of the manuscript for intellectual content: LBZ, KFS. All authors approved the final version of the paper.*

Conflicts of interest: *The authors declare that there are no conflicts of interest associated with this manuscript.*

Financial support: *This study was supported by the National Natural Science Foundation of China, No. 81771222 (to LLS); the Natural Science Foundation of Guangdong Province of China, No. 2019A1515011316 (to LLS); the National Key Research and Development Program of China, Stem Cell and Translational Research, No. 2017YFA0105102 (to LLS); the Guangzhou Science and Technology Innovation Development Special Fund Project of China, No. 201804010212 (to LLS); the Program of Introducing Talents of Discipline to Universities of China, No. B14036 (to KFS). The funding sources had no role in study conception and design, data analysis or interpretation, paper writing or deciding to submit this paper for publication.*

Institutional review board statement: *All experimental procedures and protocols were approved by Laboratory Animal Ethics Committee of Jinan University of China (approval No. 20170228010) on February 28, 2017. The cell experiments were approved by Medical Ethics Committee of the First Affiliated Hospital of Jinan University of China on February 25, 2017. The experimental procedure followed the United States National Institutes of Health Guide for the Care and Use of Laboratory Animals (NIH Publication No. 85-23, revised 1996).*

Copyright license agreement: *The Copyright License Agreement has been signed by all authors before publication.*

Data sharing statement: *Datasets analyzed during the current study are available from the corresponding author on reasonable request.*

Plagiarism check: *Checked twice by iThenticate.*

Peer review: *Externally peer reviewed.*

Open peer reviewers: *Huanxing Su, University of Macau, China; Chuntao Zhao, Cincinnati Children's Hospital Medical Center, USA.*

Additional file: *Open peer review reports 1 and 2.*

References

Berkel S, Marshall CR, Weiss B, Howe J, Roeth R, Moog U, Endris V, Roberts W, Szatmari P, Pinto D, Bonin M, Riess A, Engels H, Sprengel R, Scherer SW, Rappold GA (2010) Mutations in the SHANK2 synaptic scaffolding gene in autism spectrum disorder and mental retardation. Nat Genet 42:489-491.

Berkel S, Tang W, Trevino M, Vogt M, Obenhaus HA, Gass P, Scherer SW, Sprengel R, Schratt G, Rappold GA (2012) Inherited and de novo SHANK2 variants associated with autism spectrum disorder impair neuronal morphogenesis and physiology. Hum Mol Genet 21:344-357.

Bianchi VE, Locatelli V, Rizzi L (2017) Neurotrophic and neuroregenerative effects of GH/IGF1. Int J Mol Sci 18 doi: 10.3390/ijms18112441.

Boeckers TM, Kreutz MR, Winter C, Zuschratter W, Smalla KH, Sanmarti-Vila L, Wex H, Langnaese K, Bockmann J, Garner CC, Gundelfinger ED (2001) Proline-rich synapse-associated protein-1/cortactin binding protein 1 (ProSAP1/CortBP1) is a PDZ-domain protein highly enriched in the postsynaptic density. Ann Anat 183:101.

Castro J, Garcia RI, Kwok S, Banerjee A, Petravicz J, Woodson J, Mellios N, Tropea D, Sur M (2014) Functional recovery with recombinant human IGF1 treatment in a mouse model of Rett Syndrome. Proc Natl Acad Sci U S A 111:9941-9946.

Cheng CM, Cohen M, Tseng V, Bondy CA (2001) Endogenous IGF1 enhances cell survival in the postnatal dentate gyrus. J Neurosci Res 64:341-347.

Chilian B, Abdollahpour H, Bierhals T, Haltrich I, Fekete G, Nagel I, Rosenberger G, Kutsche K (2013) Dysfunction of SHANK2 and CHRNA7 in a patient with intellectual disability and language impairment supports genetic epistasis of the two loci. Clin Genet 84:560-565.

Chung C, Ha S, Kang H, Lee J, Um SM, Yan H, Yoo YE, Yoo T, Jung H, Lee D, Lee E, Lee S, Kim J, Kim R, Kwon Y, Kim W, Kim H, Duffney L, Kim D, Mah W, et al. (2019) Early correction of N-Methyl-D-Aspartate receptor function improves autistic-like social behaviors in adult SHANK2(-/-) mice. Biol Psychiatry 85:534-543.

Courchesne E, Pierce K, Schumann CM, Redcay E, Buckwalter JA, Kennedy DP, Morgan J (2007) Mapping early brain development in autism. Neuron 56:399-413.

Du Y, Weed SA, Xiong WC, Marshall TD, Parsons JT (1998) Identification of a novel cortactin SH3 domain-binding protein and its localization to growth cones of cultured neurons. Mol Cell Biol 18:5838-5851.

Eltokhi A, Rappold G, Sprengel R (2018) Distinct phenotypes of SHANK2 mouse models reflect neuropsychiatric spectrum disorders of human patients with SHANK2 variants. Front Mol Neurosci 11:240.

Fourie C, Vyas Y, Lee K, Jung Y, Garner CC, Montgomery JM (2018) Dietary zinc supplementation prevents autism related behaviors and striatal synaptic dysfunction in Shank3 exon 13-16 mutant mice. Front Cell Neurosci 12:374.

Fuentes-Santamaria V, Alvarado JC, Rodriguez-de la Rosa L, Juiz JM, Varela-Nieto I (2019) Neuroglial involvement in abnormal glutamate transport in the cochlear nuclei of the igf1 (-/-) mouse. Front Cell Neurosci 13:67.

Garcia-Gonzalez D, Khodosevich K, Watanabe Y, Rollenhagen A, Lubke JHR, Monyer H (2017) Serotonergic projections govern postnatal neuroblast migration. Neuron 94:534-549.

Geschwind DH (2009) Advances in autism. Annu Rev Med 60:367-380.

Grabrucker AM, Knight MJ, Proepper C, Bockmann J, Joubert M, Rowan M, Nienhaus GU, Garner CC, Bowie JU, Kreutz MR, Gundelfinger ED, Boeckers TM (2011) Concerted action of zinc and ProSAP/SHANK in synaptogenesis and synapse maturation. EMBO J 30:569-581.

Ha S, Lee D, Cho YS, Chung C, Yoo YE, Kim J, Lee J, Kim W, Kim H, Bae YC, Tanaka-Yamamoto K, Kim E (2016) Cerebellar SHANK2 regulates excitatory synapse density, motor coordination, and specific repetitive and anxiety-like behaviors. J Neurosci 36:12129-12143.

Hayashi MK, Tang C, Verpelli C, Narayanan R, Stearns MH, Xu RM, Li H, Sala C, Hayashi Y (2009) The postsynaptic density proteins Homer and SHANK form a polymeric network structure. Cell 137:159-171.

Huang G, Chen S, Chen X, Zheng J, Xu Z, Doostparast Torshizi A, Gong S, Chen Q, Ma X, Yu J, Zhou L, Qiu S, Wang K, Shi L (2019) Uncovering the functional link between SHANK3 deletions and deficiency in neurodevelopment using iPSC-derived human neurons. Front Neuroanat 13:23.

Kamijo S, Ishii Y, Horigane SI, Suzuki K, Ohkura M, Nakai J, Fujii H, Takemoto-Kimura S, Bito H (2018) A critical neurodevelopmental role for l-type voltage-gated calcium channels in neurite extension and radial migration. J Neurosci 38:5551-5566.

Kang S, Chen X, Gong S, Yu P, Yau S, Su Z, Zhou L, Yu J, Pan G, Shi L (2017) Characteristic analyses of a neural differentiation model from iPSC-derived neuron according to morphology, physiology, and global gene expression pattern. Sci Rep 7:12233.

Kathuria A, Nowosiad P, Jagasia R, Aigner S, Taylor RD, Andreae LC, Gatford NJF, Lucchesi W, Srivastava DP, Price J (2018) Stem cell-derived neurons from autistic individuals with SHANK3 mutation show morphogenetic abnormalities during early development. Mol Psychiatry 23:735-746.

Kim R, Kim J, Chung C, Ha S, Lee S, Lee E, Yoo YE, Kim W, Shin W, Kim E (2018) Cell-type-specific SHANK2 deletion in mice leads to differential synaptic and behavioral phenotypes. J Neurosci 38:4076-4092.

Lee AR, Ko KW, Lee H, Yoon YS, Song MR, Park CS (2016) Putative cell adhesion membrane protein vstm5 regulates neuronal morphology and migration in the central nervous system. J Neurosci 36:10181-10197.

Lilja J, Zacharchenko T, Georgiadou M, Jacquemet G, De Franceschi N, Peuhu E, Hamidi H, Pouwels J, Martens V, Nia FH, Beifuss M, Boeckers T, Kreienkamp HJ, Barsukov IL, Ivaska J (2017) SHANK proteins limit integrin activation by directly interacting with Rap1 and R-Ras. Nat Cell Biol 19:292-305.

Lim CS, Kim H, Yu NK, Kang SJ, Kim T, Ko HG, Lee J, Yang JE, Ryu HH, Park T, Gim J, Nam HJ, Baek SH, Wegener S, Schmitz D, Boeckers TM, Lee MG, Kim E, Lee JH, Lee YS, et al. (2017) Enhancing inhibitory synaptic function reverses spatial memory deficits in SHANK2 mutant mice. Neuropharmacology 112:104-112.

Lim L, Pakan JMP, Selten MM, Marques-Smith A, Llorca A, Bae SE, Rochefort NL, Marin O (2018) Optimization of interneuron function by direct coupling of cell migration and axonal targeting. Nat Neurosci 21:920-931.

Lim S, Naisbitt S, Yoon J, Hwang JI, Suh PG, Sheng M, Kim E (1999) Characterization of the SHANK family of synaptic proteins. Multiple genes, alternative splicing, and differential expression in brain and development. J Biol Chem 274:29510-29518.

Luo T, Liu P, Wang XY, Li LZ, Zhao LP, Huang J, Li YM, Ou JL, Peng XQ (2018) Effect of the autism-associated lncRNA SHANK2-AS on architecture and growth of neurons. J Cell Biochem doi: 10.1002/jcb.27471.

Marchetto MC, Carromeu C, Acab A, Yu D, Yeo GW, Mu Y, Chen G, Gage FH, Muotri AR (2010) A model for neural development and treatment of Rett syndrome using human induced pluripotent stem cells. Cell 143:527-539.

Mateos-Aparicio P, Rodriguez-Moreno A (2020) Calcium dynamics and synaptic plasticity. Adv Exp Med Biol 1131:965-984.

Monteiro P, Feng G (2017) SHANK proteins: roles at the synapse and in autism spectrum disorder. Nat Rev Neurosci 18:147-157.

Neher E, Sakaba T (2008) Multiple roles of calcium ions in the regulation of neurotransmitter release. Neuron 59:861-872.

Pan YH, Wu N, Yuan XB (2019) Toward a better understanding of neuronal migration deficits in autism spectrum disorders. Front Cell Dev Biol 7:205.

Pappas AL, Bey AL, Wang X, Rossi M, Kim YH, Yan H, Porkka F, Duffney LJ, Phillips SM, Cao X, Ding JD, Rodriguiz RM, Yin HH, Weinberg RJ, Ji RR, Wetsel WC, Jiang YH (2017) Deficiency of SHANK2 causes mania-like behavior that responds to mood stabilizers. JCI Insight 2:e92052.

Pchitskaya E, Popugaeva E, Bezprozvanny I (2018) Calcium signaling and molecular mechanisms underlying neurodegenerative diseases. Cell Calcium 70:87-94.

Peter S, Ten Brinke MM, Stedehouder J, Reinelt CM, Wu B, Zhou H, Zhou K, Boele HJ, Kushner SA, Lee MG, Schmeisser MJ, Boeckers TM, Schonewille M, Hoebeek FE, De Zeeuw CI (2016) Dysfunctional cerebellar Purkinje cells contribute to autism-like behaviour in SHANK2-deficient mice. Nat Commun 7:12627.

Sala C, Piech V, Wilson NR, Passafaro M, Liu G, Sheng M (2001) Regulation of dendritic spine morphology and synaptic function by SHANK and Homer. Neuron 31:115-130.

Sala C, Vicidomini C, Bigi I, Mossa A, Verpelli C (2015) SHANK synaptic scaffold proteins: keys to understanding the pathogenesis of autism and other synaptic disorders. J Neurochem 135:849-858.

Schmeisser MJ, Ey E, Wegener S, Bockmann J, Stempel AV, Kuebler A, Janssen AL, Udvardi PT, Shiban E, Spilker C, Balschun D, Skryabin BV, Dieck St, Smalla KH, Montag D, Leblond CS, Faure P, Torquet N, Le Sourd AM, Toro R, et al. (2012) Autistic-like behaviours and hyperactivity in mice lacking ProSAP1/SHANK2. Nature 486:256-260.

Scolnick JA, Cui K, Duggan CD, Xuan S, Yuan XB, Efstratiadis A, Ngai J (2008) Role of IGF signaling in olfactory sensory map formation and axon guidance. Neuron 57:847-857.

Shcheglovitov A, Shcheglovitova O, Yazawa M, Portmann T, Shu R, Sebastiano V, Krawisz A, Froehlich W, Bernstein JA, Hallmayer JF, Dolmetsch RE (2013) SHANK3 and IGF1 restore synaptic deficits in neurons from 22q13 deletion syndrome patients. Nature 503:267-271.

Sheng M, Kim E (2000) The SHANK family of scaffold proteins. J Cell Sci 113:1851-1856.

Shi R, Redman P, Ghose D, Hwang H, Liu Y, Ren X, Ding LJ, Liu M, Jones KJ, Xu W (2017) SHANK proteins differentially regulate synaptic transmission. eNeuro doi: 10.1523/ENEURO.0163-15.2017.

Tu JC, Xiao B, Naisbitt S, Yuan JP, Petralia RS, Brakeman P, Doan A, Aakalu VK, Lanahan AA, Sheng M, Worley PF (1999) Coupling of mGluR/Homer and PSD-95 complexes by the SHANK family of postsynaptic density proteins. Neuron 23:583-592.

Turner TN, Coe BP, Dickel DE, Hoekzema K, Nelson BJ, Zody MC, Kronenberg ZN, Hormozdiari F, Raja A, Pennacchio LA, Darnell RB, Eichler EE (2017) Genomic patterns of de novo mutation in simplex autism. Cell 171:710-722.

Wang L, Wang L, Huang W, Su H, Xue Y, Su Z, Liao B, Wang H, Bao X, Qin D, He J, Wu W, So KF, Pan G, Pei D (2013) Generation of integration-free neural progenitor cells from cells in human urine. Nat Methods 10:84-89.

Wegener S, Buschler A, Stempel AV, Kang SJ, Lim CS, Kaang BK, Shoichet SA, Manahan-Vaughan D, Schmitz D (2018) Defective synapse maturation and enhanced synaptic plasticity in SHANK2 deltaex7(-/-) mice. eNeuro doi: 10.1523/ENEURO.0398-17.2018.

Wegiel J, Kuchna I, Nowicki K, Imaki H, Wegiel J, Marchi E, Ma SY, Chauhan A, Chauhan V, Bobrowicz TW, de Leon M, Louis LA, Cohen IL, London E, Brown WT, Wisniewski T (2010) The neuropathology of autism: defects of neurogenesis and neuronal migration, and dysplastic changes. Acta Neuropathol 119:755-770.

Won H, Lee HR, Gee HY, Mah W, Kim JI, Lee J, Ha S, Chung C, Jung ES, Cho YS, Park SG, Lee JS, Lee K, Kim D, Bae YC, Kaang BK, Lee MG, Kim E (2012) Autistic-like social behaviour in SHANK2-mutant mice improved by restoring NMDA receptor function. Nature 486:261-265.

Zaslavsky K, Zhang WB, McCready FP, Rodrigues DC, Deneault E, Loo C, Zhao M, Ross PJ, El Hajjar J, Romm A, Thompson T, Piekna A, Wei W, Wang Z, Khattak S, Mufteev M, Pasceri P, Scherer SW, Salter MW, Ellis J (2019) SHANK2 mutations associated with autism spectrum disorder cause hyperconnectivity of human neurons. Nat Neurosci 22:556-564.

Zhou Y, Kaiser T, Monteiro P, Zhang X, Van der Goes MS, Wang D, Barak B, Zeng M, Li C, Lu C, Wells M, Amaya A, Nguyen S, Lewis M, Sanjana N, Zhou Y, Zhang M, Zhang F, Fu Z, Feng G (2016) Mice with Shank3 mutations associated with ASD and schizophrenia display both shared and distinct defects. Neuron 89:147-162.

P-Reviewers: Su H, Zhao C; C-Editor: Zhao M; S-Editors: Wang J, Li CH; L-Editors: Patel B, Haase R, Qiu Y, Song LP; T-Editor: Jia Y